Classically emulated digital quantum simulation of the Schwinger model with a topological term via adiabatic state preparation

Bipasha Chakraborty,[1,*] Masazumi Honda[1,†] Taku Izubuchi,[2,3,‡] Yuta Kikuchi[3,§] and Akio Tomiya[3,‖]

[1]*Department of Applied Mathematics and Theoretical Physics, Centre for Mathematical Sciences,*
Wilberforce Road, Cambridge CB3 0WA, United Kingdom
[2]*Physics Department, Brookhaven National Laboratory, Upton, New York 11973, USA*
[3]*RIKEN BNL Research center, Brookhaven National Laboratory, Upton, New York 11973, USA*

We designed a protocol for digital quantum computation of a gauge theory with a topological term in Minkowski spacetime, which is practically inaccessible by standard lattice Monte Carlo simulations. We focus on $1 + 1$ dimensional quantum electrodynamics with the θ term known as the Schwinger model and test our protocol for this on an IBM simulator. We construct the true vacuum state of a lattice Schwinger model using adiabatic state preparation which, in turn, allows us to compute an expectation value of the fermion mass operator with respect to the vacuum. Upon taking a continuum limit we find that our result in the massless case agrees with the known exact result. In the massive case, we find an agreement with mass perturbation theory in the small-mass regime and deviations in the large-mass regime. We estimate computational costs required to take a reasonable continuum limit. Our results imply that digital quantum simulation appears a promising tool to explore nonperturbative aspects of gauge theories with real time and topological terms.

I. INTRODUCTION

Gauge theory plays a central role in understanding our universe as all the known fundamental forces are described in the framework of gauge theory. Quantum chromodynamics (QCD) is the gauge theory describing the strong interaction among quarks and gluons. Since QCD is asymptotically free, we need a nonperturbative treatment at low energy to interpolate perturbative picture of quarks/gluons and physics of hadrons. The only successful first-principle approach to handle this is lattice QCD in which we conventionally consider QCD on 4D Euclidean spacetime and discretize the spacetime by lattice to make the path integral finite dimensional. Evaluating the regularized path integral numerically and taking a continuum limit carefully, one can study non-perturbative phenomena such as confinement and chiral symmetry breaking, and reproduce the correct hadron

*bc335@damtp.cam.ac.uk
†masazumi.honda@yukawa.kyoto-u.ac.jp
‡izubuchi@quark.phy.bnl.gov
§yuta.kikuchi@riken.jp
‖akio.tomiya@riken.jp

spectrum [1–4]. Numerical integration of the path integral in lattice-field theory is usually done by the Markov Chain Monte Carlo method which regards Boltzmann weight as a probability. Therefore, it encounters a problem when the integrand is nonreal positive and highly oscillating so that sampling becomes much less efficient. This problem, known as the sign problem physically happens, e.g., when we have topological terms [5], chemical potentials [6], or real time [7]. All of the above cases are crucial to understand our universe and therefore, an efficient way to explore the above situations is highly demanded [3–7].

There are various approaches to challenge the sign problem within the framework of the path integral formalism [6]; however, there is limited success as the sign problem gets stronger. One may wonder if it is possible to attack gauge theories with the sign problem by switching to the Hamiltonian formalism where the sign problem is absent from the beginning. Instead, we have to regularize infinite-dimensional Hilbert space and play with huge vector space whose dimension is typically more than exponential of spatial volume in the unit of UV cutoff. It seems beyond the capacity of current/near-future supercomputers when spacetime dimension is not low. However, it is reasonable to expect that *quantum computers* do this job in the not so distant future. Anticipating growth of quantum computational resources, it is worth to develop methods to analyze gauge theories suitable for quantum computers to prepare for the coming era of quantum supremacy [8,9]. It is particularly

important to identify suitable algorithms and estimate computational resources required to take a reasonable continuum limit.

In this paper, we design a protocol for a *digital quantum simulation* of a gauge theory with a topological term on Minkowski spacetime which is practically inaccessible by the standard Monte Carlo approach. We focus on the Schwinger model with the θ term [10–13], which is $1 + 1$ dimensional $U(1)$ gauge theory coupled to a Dirac fermion described by the Lagrangian,

$$
\mathcal{L}_0 = -\frac{1}{4} F_{\mu\nu} F^{\mu\nu} + \frac{g\theta}{4\pi} \epsilon_{\mu\nu} F^{\mu\nu}
$$
$$
+ \, i\bar{\psi}\gamma^\mu(\partial_\mu + igA_\mu)\psi - m\bar{\psi}\psi, \quad (1)
$$

where $\gamma^0 = \sigma^3$, $\gamma^1 = i\sigma^2$, $\gamma^5 = \gamma^0\gamma^1$, and $F_{\mu\nu} = \partial_\mu A_\nu - \partial_\nu A_\mu$. The physical parameters of this model are the gauge coupling g, topological angle θ, and fermion mass m. We discretize the space by lattice, keeping time continuous and work in Hamiltonian formalism. Then, we construct the true vacuum of the lattice Schwinger model at finite (g, θ, m) by a digital quantum simulation via adiabatic state preparation and compute the vacuum expectation value (VEV) of the fermion mass operator $\bar{\psi}\psi$. We take a continuum limit and find that our result in the massless case agrees with the exact result known in literature [14–17]. In the massive case, we find an agreement with mass perturbation theory [18,19] for small m and deviations for large m. Our results imply that digital quantum simulation is already a useful tool to explore nonperturbative aspects of gauge theories with topological terms on Minkowski spacetime even in current computational resource. Here we use a classical simulator for quantum hardware rather than real quantum computers for the purpose of designing quantum algorithms for gauge theories. Its implementations on a real quantum device is left as future work, that is, another vital task especially in the forthcoming Noisy Intermediate-Scale Quantum (NISQ) era [20].

Many efforts have already been made in designing and implementing digital quantum simulations of quantum-field theories [21–41] as well as analog quantum simulations [42–55]. In particular, the Schwinger model provides an ideal laboratory for developing quantum algorithms with limited quantum resources foreseeing larger-scale digital quantum simulations of various gauge theories. So far, applications of quantum algorithms for the Schwinger model are limited to $\theta = 0$, and performed with a free vacuum and quenching evolution [28,29,33,39,56], while analog quantum simulations have been implemented in [51,55].

The present work demonstrates how to construct the true vacuum in an interacting gauge theory with the topological term by a digital quantum simulation. We believe that our results open up potential applications of digital quantum simulation to quantum-field theory since the preparation of true ground state is indispensable to

calculate various observables such as scattering amplitudes nonperturbatively.[1]

II. SCHWINGER MODEL AS QUBITS

First, we rewrite the lattice Schwinger model in terms of spin operators which act on the Hilbert space represented by qubits according to [62]. Instead of directly analyzing the system with the Lagrangian (1), we consider the Lagrangian obtained by the chiral rotation $\psi \to e^{i\frac{\theta}{2}\gamma_5}\psi$ to absorb the θ term via the transformation of the path integral measure [63]. Therefore, we can study the same physics by the Lagrangian,

$$
\mathcal{L} = -\frac{1}{4} F_{\mu\nu} F^{\mu\nu} + i\bar{\psi}\gamma^\mu(\partial_\mu + igA_\mu)\psi - m\bar{\psi}e^{i\theta\gamma^5}\psi. \quad (2)
$$

In the temporal gauge $A_0 = 0$, the Hamiltonian of this model is

$$
H = \int dx \left[-i\bar{\psi}\gamma^1(\partial_1 + igA_1)\psi + m\bar{\psi}e^{i\theta\gamma^5}\psi + \frac{1}{2}\Pi^2 \right], \quad (3)
$$

where $\Pi \equiv \dot{A}^1$ is the conjugate momentum of A^1. The gauge invariance of physical Hilbert space is guaranteed by imposing the Gauss law:

$$
0 = -\partial_1\Pi - g\bar{\psi}\gamma^0\psi. \quad (4)
$$

A. Lattice theory with staggered fermion

To implement a quantum simulation algorithm, we need a regularization to make the Hilbert space finite dimensional. For the Schwinger model, this is done just by placing the theory on a lattice and imposing the Gauss law[2] [29]. Let us consider the theory on 1D spatial lattice with N sites and lattice spacing a keeping the time continuous. Using the staggered fermion [64,65], the lattice Hamiltonian is given by[3]

$$
H = -i \sum_{n=1}^{N-1} \left(w - (-1)^n \frac{m}{2}\sin\theta \right) [\chi_n^\dagger e^{i\phi_n}\chi_{n+1} - \text{H.c.}]
$$
$$
+ \, m\cos\theta \sum_{n=1}^{N} (-1)^n \chi_n^\dagger \chi_n + J \sum_{n=1}^{N-1} L_n^2, \quad (5)
$$

where $w = 1/(2a)$ and $J = g^2a/2$. We have rescaled the gauge operators as $\phi_n \leftrightarrow -agA^1(x)$ and $L_n \leftrightarrow -\Pi(x)/g$,

---

[1]Schwinger model with the θ term has been studied by other approaches without using quantum computing in [57–61].

[2]This is true for open boundary condition while there is a remaining gauge degree of freedom for periodic boundary condition.

[3]Note that staggered fermion in $1 + 1$ dimensions in Hamilton formalism has only one taste.

where ϕ_n lives on a site n while L_n lives on a link between sites n and $n + 1$. A two-component Dirac fermion $\psi(x) = (\psi_u(x), \psi_d(x))^\mathsf{T}$ is translated into a pair of neighboring one-component fermions according to the correspondence (see Appendix A for details):

$$\frac{\chi_n}{\sqrt{a}} \leftrightarrow \begin{cases} \psi_u(x) & n: \text{ even} \\ \psi_d(x) & n: \text{ odd} \end{cases}. \qquad (6)$$

They satisfy the (anti-)commutation relations

$$\{\chi_n^\dagger, \chi_m\} = \delta_{mn}, \quad \{\chi_n, \chi_m\} = 0, \quad [\phi_n, L_m] = \mathrm{i}\delta_{mn}, \qquad (7)$$

and the Gauss law on the lattice is

$$L_n - L_{n-1} = \chi_n^\dagger \chi_n - \frac{1 - (-1)^n}{2}. \qquad (8)$$

B. Mapping to spin system

We rewrite the system in terms of spin variables in three steps. Firstly, we perform the Jordan-Wigner transformation [66], which maps the fermions to spin variables as

$$\chi_n = \left(\prod_{\ell < n} -\mathrm{i}Z_\ell\right) \frac{X_n - \mathrm{i}Y_n}{2}, \qquad (9)$$

where (X_n, Y_n, Z_n) stands for the Pauli matrices $(\sigma^1, \sigma^2, \sigma^3)$ at site n. Secondly, we specify a boundary condition and solve the Gauss law. We impose an open boundary condition which restricts L_n to a constant at the boundary. Solving the Gauss law, we rewrite L_n in terms of the spin variables as

$$L_n = L_0 + \frac{1}{2}\sum_{\ell=1}^{n}(Z_\ell + (-1)^\ell), \qquad (10)$$

where the constant L_0 specifies our boundary condition. The Schwinger model with (θ, L_0) is equivalent to the one with $(\theta + 2\pi L_0, 0)$ [12] and therefore we can take $L_0 = 0$ without loss of generality. Finally, we can eliminate ϕ_n by the redefinition[4] $\chi_n \to \prod_{\ell < n}[e^{-\mathrm{i}\phi_\ell}]\chi_n$.

Thus, the lattice Schwinger model is purely described in terms of the spin variables:

$$H = H_{ZZ} + H_\pm + H_Z, \qquad (11)$$

where

---

[4]If we took a periodic boundary condition, then L_0 was dynamical and one of ϕ_n's could not be eliminated by the redefinition.

$$H_{ZZ} = \frac{J}{2}\sum_{n=2}^{N-1}\sum_{1 \leq k < \ell \leq n} Z_k Z_\ell,$$

$$H_\pm = \frac{1}{2}\sum_{n=1}^{N-1}\left(w - (-1)^n\frac{m}{2}\sin\theta\right)[X_n X_{n+1} + Y_n Y_{n+1}],$$

$$H_Z = \frac{m\cos\theta}{2}\sum_{n=1}^{N}(-1)^n Z_n - \frac{J}{2}\sum_{n=1}^{N-1}(n \bmod 2)\sum_{\ell=1}^{n} Z_\ell, \quad (12)$$

up to irrelevant constant terms. Note that the nonlocal interactions in H_{ZZ} show up as a consequence of solving the Gauss law constraint. For the formulation based on (1), see Appendix B.

III. ADIABATIC PREPARATION OF VACUUM

We study the VEV of the mass operator:

$$\langle\bar{\psi}(x)\psi(x)\rangle = \langle\text{vac}|\bar{\psi}(x)\psi(x)|\text{vac}\rangle, \qquad (13)$$

where $|\text{vac}\rangle$ is the ground state of the full Hamiltonian H. Here, instead of directly studying the local operator $\bar{\psi}(x)\psi(x)$, we analyze the operator averaged over space:

$$\frac{1}{2Na}\langle\text{vac}|\sum_{n=1}^{N}(-1)^n Z_n|\text{vac}\rangle, \qquad (14)$$

whose continuum limit is the same as $\langle\bar{\psi}(x)\psi(x)\rangle$ by translational invariance.

We prepare the vacuum state $|\text{vac}\rangle$ using the adiabatic theorem as follows. We first choose an initial Hamiltonian H_0 of a simple system such that its ground state $|\text{vac}\rangle_0$ is unique and known. Next, we consider the following time evolution of $|\text{vac}\rangle_0$:

$$\mathcal{T}\exp\left(-\mathrm{i}\int_0^T dt H_\text{A}(t)\right)|\text{vac}\rangle_0, \qquad (15)$$

where $\mathcal{T}\exp$ denotes a time-ordered exponential. The adiabatic Hamiltonian $H_\text{A}(t)$ is an Hermitian operator satisfying

$$H_\text{A}(0) = H_0, \qquad H_\text{A}(T) = H. \qquad (16)$$

The adiabatic theorem claims that, if the system described by the Hamiltonian $H_\text{A}(t)$ is gapped and has a unique ground state, then the ground state of H is obtained by the time evolution

$$|\text{vac}\rangle = \lim_{T \to \infty}\mathcal{T}\exp\left(-\mathrm{i}\int_0^T dt H_\text{A}(t)\right)|\text{vac}\rangle_0. \qquad (17)$$

In practice, we take finite T and discretize the integral, and therefore we can obtain only an approximation of the vacuum. This implies that an expectation value of an

operator under the approximate vacuum has intrinsic systematic errors. In Appendix D, we discuss how we estimate the systematic errors.

In our simulation, we take the initial Hamiltonian H_0 as

$$H_0 = H_{ZZ} + H_Z|_{m \to m_0, \theta \to 0}, \qquad (18)$$

where $m_0 \in \mathbb{R}_{\geq 0}$ can be arbitrary in principle; however, it is chosen so that systematic errors become small. The ground state of H_0 is

$$|\text{vac}\rangle_0 = |0\rangle \otimes |1\rangle \otimes \cdots \otimes |0\rangle \otimes |1\rangle, \qquad (19)$$

where $Z|0\rangle = |0\rangle$ and $Z|1\rangle = -|1\rangle$. In order to evolve it into the desired vacuum state we choose the following adiabatic Hamiltonian:

$$H_A(t) = H_{ZZ} + H_{\pm,A}(t) + H_{Z,A}(t), \qquad (20)$$

with $H_{\pm,A}$ and $H_{Z,A}$ obtained by replacing the parameters of $H_\pm$ and H_Z in the Hamiltonian (11) as

$$w \to \frac{t}{T}w, \qquad \theta \to \frac{t}{T}\theta, \qquad m \to \left(1 - \frac{t}{T}\right)m_0 + \frac{t}{T}m. \quad (21)$$

We take finite T and approximate the time evolution (17) by [67,68]

$$|\text{vac}\rangle \simeq U(T)U(T - \delta t) \cdots U(2\delta t)U(\delta t)|\text{vac}\rangle_0, \qquad (22)$$

where $U(t) = e^{-iH_A(t)\delta t}$ and $\delta t = \frac{T}{M}$ with a large positive integer M. The most naive way to approximate the operator $U(t)$ is

$$U(t) = e^{-iH_{ZZ}\delta t}e^{-iH_{\pm,A}(t)\delta t}e^{-iH_{Z,A}(t)\delta t} + \mathcal{O}(\delta t^2). \qquad (23)$$

While we use this approximation for $\theta = 0$ with $(T, \delta t) = (100, 0.1)$, we use an improved version of (23) for $\theta \neq 0$ with $(T, \delta t) = (150, 0.3)$ by using

$$U(t) = e^{-iH_{\pm,A}(t)\frac{\delta t}{2}}e^{-iH_{ZZ}\delta t}e^{-iH_{Z,A}(t)\delta t}e^{-iH_{\pm,A}(t)\frac{\delta t}{2}} + \mathcal{O}(\delta t^3), \qquad (24)$$

which is detailed in Appendix E. We implement all the operators in the time evolution by combinations of quantum elementary gates provided by IBM Qiskit library (see Appendix C). Finally, in the process of measurement of the mass operator, we take the number of shots to be 10^6 in all the data points. This induces statistical errors in addition to the systematic errors.

A. Estimation of number of gates

Here we have used a classical simulator for quantum hardware to see how our algorithm practically works and grasp a future prospect on applications of real quantum computers to quantum-field theory. The maximal number of qubits in our simulation is 16, which is not so big even in current technology. While this is quite encouraging, the adiabatic preparation of state adopted here requires a large number of gates: our quantum circuit for 16 qubits without improvement of Trotter decomposition has about 250 single-qubit gates and 270 two-qubit gates at each time step which has been repeated about 1000 times. This would make much noise and be hard to perform stable simulations when we implement our simulation on NISQ devices.

IV. RESULTS

A. Massless case

Let us first focus on the massless case and compare with the exact result in the continuum theory [14–17],

$$\langle \bar{\psi}(x)\psi(x)\rangle = -\frac{e^\gamma}{2\pi^{3/2}}g \approx -0.160g, \qquad (25)$$

where γ is the Euler-Mascheroni constant. Note that the θ parameter is irrelevant in this case since our lattice Hamiltonian is independent of θ for $m = 0$. We take a physical limit for fixed physical parameters (g, m, θ) in two steps: (i) Take infinite volume limit. Namely, for fixed $w = 1/2a$ and the physical parameters, we compute the observables for various N's and then extrapolate them to $N \to \infty$ with quadratic polynomial in $1/N$. Repeating this for multiple values of w, we obtain data of infinite volume limit for various lattice spacing a at fixed physical parameters. This step is illustrated in Fig. 1 (left). (ii) Extrapolate the data of the infinite volume limit to the continuum limit $a \to 0$ with quadratic polynomial in ag. This procedure is demonstrated in Fig. 1 (right).

Repeating the above procedures, we have obtained g dependence of the mass operator in the continuum limit as shown in Fig. 2. We see that our result agrees with the exact result. Note that the massless case cannot be easily explored by the standard Monte Carlo approach because computational cost to evaluate effects of fermions in the standard approach is $O((am)^{-1})$ [69]. This point is another advantage of our approach over the standard Monte Carlo approach.

B. Massive case

Next, we consider the massive case. For this case, there is a result by mass perturbation theory [18,19]:

$$\langle \bar{\psi}(x)\psi(x)\rangle \approx -0.160g + 0.322m\cos\theta, \qquad (26)$$

up to $\mathcal{O}(m^2)$. There is a subtlety in comparison with this result: the observable is UV divergent logarithmically and
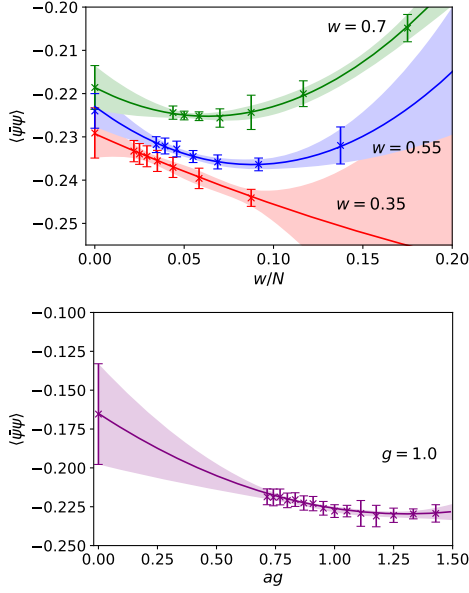
FIG. 1. (Top) Infinite volume limits for some values of w at $g = 1$, $m = 0$, $\theta = 0$. For each w, we compute the VEV of the mass operator $\langle \bar{\psi}\psi \rangle$ for $N = [4, 16]$ and extrapolate it to $N \to \infty$ by fitting the data to a quadratic polynomial of w/N shown by the solid curves. The error bars in the data points and error bands include both statistical and systematic errors. (Bottom) Continuum limits at $m = 0$, $\theta = 0$ for $g = 1$. The solid curve shows the fit function which is a quadratic polynomial in ag. The error bars and the error band take account of the extrapolation errors as well as the statistical and other systematic errors.
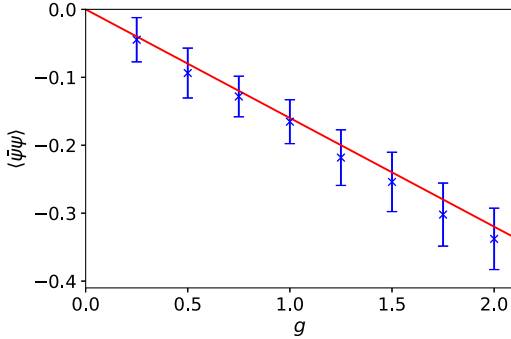
FIG. 2. The VEV of the mass operator for $m = 0$ is plotted against coupling constant g. The red solid line shows the exact result, which is approximately $-0.160g$. The error bars take account of extrapolation errors as well as the statistical and systematic errors.

we need to regularize it. Here we adopt a lattice counterpart of a regularization used in [18] which is a subtraction of the free-theory result. Specifically, we take infinite volume limit without subtraction as in Fig. 1 (left) but subtract the result at $J = 0$ and $N \to \infty$ in taking the continuum limit:

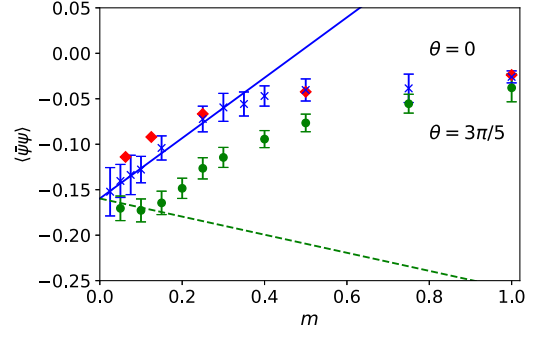

FIG. 3. The VEV of the mass operator at $g = 1$ is plotted against the mass m for $\theta = 0$ (blue ×'s) and $\theta = 3\pi/5$ (green circles). The red diamonds show the numerical result at $\theta = 0$ obtained by the tensor network approach in [70]. The lines show the result (26) of the mass perturbation. The error bars are fitting errors in taking the continuum limit.

$$\langle \bar{\psi}(x)\psi(x) \rangle_{\text{free}} = -\frac{m \cos\theta}{\pi\sqrt{1 + (ma \cos\theta)^2}} K(z),$$

$$K(z) = \int_0^{\frac{\pi}{2}} \frac{dt}{\sqrt{1 - z\sin^2 t}}, \qquad z = \frac{1 - (ma \sin\theta)^2}{1 + (ma \cos\theta)^2}.$$

$$(27)$$

In other words, we replace $\langle \bar{\psi}\psi \rangle$ in Fig. 1 (right) by $\langle \bar{\psi}\psi \rangle - \langle \bar{\psi}\psi \rangle_{\text{free}}$ for the massive case.

In Fig. 3, we plot our result in the continuum limit for $(g, \theta) = (1, 0)$ and $(g, \theta) = (1, 3\pi/5)$ against m, and compare with the mass perturbation theory (26). We see that our result agrees with the mass perturbation theory in small-mass regime for the both values of θ. As increasing mass, it deviates from (26) and finally approaches zero. This large-mass asymptotic behavior is expected since the large-mass limit should be the same as the free-theory result which we have subtracted. Our result for $\theta = 0$ also agrees with previous numerical result obtained by tensor network approach [70]. Furthermore, we compare θ dependence of the VEV of the mass operator for the parameters in Fig. 4, for which the mass perturbation (26) is expected to be well behaved: $(g, m) = (1.0, 0.1)$.[5] We see that our data agree with the mass perturbation for most values of θ while we get small deviations around $\theta = \pi$ within our current accuracy. Thus, we conclude that our approach practically works well for nonzero (g, m, θ).

V. SUMMARY AND DISCUSSIONS

In this paper, we have designed the protocol for the digital quantum simulation of the Schwinger model with

---

[5]It is expected that the Schwinger model at $\theta = \pi$ has a critical point at $m \simeq 0.33g$ and first-order phase transition associated with spontaneous breaking of charge conjugation symmetry (or equivalently parity) for larger m. Therefore, we are not passing any phase transition point in Fig. 4.
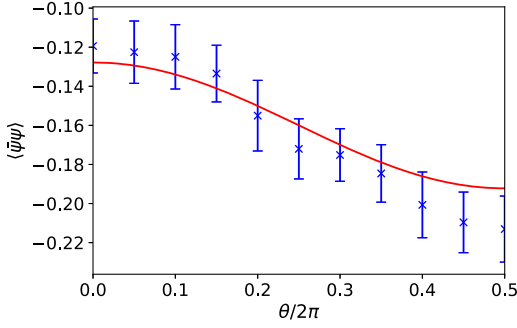
FIG. 4. The VEV of the mass operator at $g = 1$ and $m = 0.1$ is plotted against $\theta/2\pi$ (blue symbols). The curve shows the result (26) of the mass perturbation with fixed g and m.

the θ term as the first example of applications of quantum algorithms for gauge theory with topological terms. We have converted the Schwinger model to the spin system on the spatial lattice and then constructed the true vacuum state of the model using adiabatic state preparation. We have computed VEV of the fermion mass operator, taken the continuum limit, and found agreement with the results in literature. Our results imply that digital quantum simulation is already tool to explore nonperturbative aspects of gauge theories with real time and topological terms.

Our estimation for number of gates in our simulation hints at large noise and difficulty performing stable simulations when implemented on NISQ devices. Therefore, it is important to save the number of gates and reduce noise by improving the algorithm. One way is to improve the Suzuki-Trotter decomposition so that we can take smaller time steps M to achieve similar errors. Another way is to change the adiabatic Hamiltonian (20) so that we can take smaller adiabatic time T. In principle, the adiabatic Hamiltonian $H_A(t)$ can be any Hermitian operator satisfying 16)) as long as the system during the adiabatic process is gapped and has a unique ground state.

There are various interesting applications and generalization of our work. An obvious application is to compute other observables in the Schwinger model. Specifically, the massive Schwinger model is known to exhibit confinement [71] and therefore it would be interesting to explore physics of confinement in a situation where standard Monte Carlo approach is inapplicable. Another interesting direction is to apply our methods to other theories. Our formulation to rewrite gauge theory in terms of qubits can be directly applied to any $1+1$ dimensional $U(1)$ gauge theory coupled to fermions. It would also be interesting to implement a digital quantum simulation of $1+1$ dimensional non-Abelian gauge theories.

ACKNOWLEDGMENTS

APPENDIX A: OPERATOR CORRESPONDENCE BETWEEN DIRAC AND STAGGERED FERMIONS

The Dirac fermion operator $\psi(x) = (\psi_u(x), \psi_d(x))^{\mathsf{T}}$ is translated into those of staggered fermions as follows [64,65]:

$$\frac{\chi_n}{\sqrt{a}} \leftrightarrow \begin{cases} \psi_u(x) & n\colon \text{even} \\ \psi_d(x) & n\colon \text{odd} \end{cases}. \tag{A1}$$

Here, we see how the bilinear operators $\bar{\psi}\gamma^1\partial_1\psi$, $\bar{\psi}\psi$, and $\bar{\psi}\gamma^5\psi$ are written in terms of the staggered fermions. We start with the fermion kinetic operator $\bar{\psi}\gamma^1\partial_1\psi$:

$$\bar{\psi}(x)\gamma^1\partial_1\psi(x)$$
$$= \psi_u^\dagger(x)\frac{\psi_d(x+1) - \psi_d(x)}{2a} + \psi_d^\dagger(x)\frac{\psi_u(x) - \psi_u(x-1)}{2a},$$
$$= \frac{1}{2a^2}[\chi_{2x}^\dagger(\chi_{2x+1} - \chi_{2x-1}) + \chi_{2x-1}^\dagger(\chi_{2x} - \chi_{2x-2})]. \tag{A2}$$

Thus, we arrive at the following expression:

$$a\sum_{x=1}^{N/2}\bar{\psi}(x)\gamma^1\partial_1\psi(x) = \frac{1}{2a}\sum_{n=1}^{N-1}[\chi_n^\dagger\chi_{n+1} - \chi_{n+1}^\dagger\chi_n]. \tag{A3}$$

Next, we convert the fermion mass operator $\bar{\psi}\psi$:

$$\bar{\psi}(x)\psi(x) = \psi_u^\dagger(x)\psi_u(x) - \psi_d^\dagger(x)\psi_d(x),$$
$$= \frac{1}{a}[\chi_{2x}^\dagger\chi_{2x} - \chi_{2x-1}^\dagger\chi_{2x-1}], \tag{A4}$$

which leads us to

$$a\sum_{x=1}^{N/2}\bar{\psi}(x)\psi(x) = \sum_{n=1}^{N}(-1)^n\chi_n^\dagger\chi_n. \tag{A5}$$

Finally, we consider the pseudo-mass operator $\bar{\psi}\gamma_5\psi$. Since it is a fermion bilinear operator involving off-diagonal matrix, the conversion to staggered fermion yields a hopping term connecting even and odd sites:

$$\bar{\psi}(x)\gamma_5\psi(x) = \psi_u^\dagger(x)\psi_d(x) - \psi_d^\dagger(x)\psi_u(x)$$

$$\approx \frac{1}{2}[\psi_u^\dagger(x)\psi_d(x) - \psi_d^\dagger(x)\psi_u(x)]$$

$$+ \frac{1}{2}[\psi_u^\dagger(x)\psi_d(x+1) - \psi_d^\dagger(x+1)\psi_u(x)]$$

$$= -\frac{1}{2a}[\chi_{2x-1}^\dagger\chi_{2x} - \chi_{2x}^\dagger\chi_{2x-1}]$$

$$+ \frac{1}{2a}[\chi_{2x}^\dagger\chi_{2x+1} - \chi_{2x+1}^\dagger\chi_{2x}], \qquad (A6)$$

where we have used $\psi_d(x+1) = \psi_d(x) + \mathcal{O}(a)$ to modify the operator, which recovers the original one in the continuum limit $a \to 0$. Thus, the pseudo-mass operator is rewritten as

$$\sum_{x=1}^{N/2} \bar{\psi}(x)\gamma_5\psi(x) = \frac{1}{2}\sum_{n=1}^{N-1}(-1)^n[\chi_n^\dagger\chi_{n+1} - \chi_{n+1}^\dagger\chi_n]. \qquad (A7)$$

APPENDIX B: ALTERNATIVE METHOD: WITHOUT CHIRAL ROTATION

Here we rewrite the Schwinger model based on the Lagrangian (1) without the chiral rotation in terms of the spin variables. In the temporal gauge, conjugate momentum of A^1 is

$$\Pi = \frac{\partial\mathcal{L}}{\partial\dot{A}^1} = \dot{A}^1 + \frac{g\theta}{2\pi}, \qquad (B1)$$

and therefore the Hamiltonian is

$$H = \int dx \left[-i\bar{\psi}\gamma^1(\partial_1 + igA_1)\psi + m\bar{\psi}\psi + \frac{1}{2}\left(\Pi - \frac{g\theta}{2\pi}\right)^2 \right]. \qquad (B2)$$

Using the staggered fermion, the lattice Hamiltonian is given by

$$H = -iw\sum_{n=1}^{N-1}[\chi_n^\dagger e^{i\phi_n}\psi_{n+1} - \chi_{n+1}^\dagger e^{-i\phi_n}\chi_n]$$

$$+ m\sum_{n=1}^{N}(-1)^n\chi_n^\dagger\chi_n + J\sum_{n=1}^{N-1}\left(L_n + \frac{\theta}{2\pi}\right)^2, \qquad (B3)$$

where L_n corresponds to $-\Pi(x)/g$ and the operators satisfy the commutation relations (7) as well as the Gauss law (8) on physical states. Applying the Jordan-Wigner transformation (9), taking the open boundary condition with constant L_0, and solving the Gauss law, we obtain the lattice Hamiltonian:

$$H = w\sum_{n=1}^{N-1}[\sigma_n^+\sigma_{n+1}^- + \text{H.c.}] + \frac{m}{2}\sum_{n=1}^{N}(-1)^n Z_n$$

$$+ J\sum_{n=1}^{N-1}\left[L_0 + \frac{\theta}{2\pi} + \frac{1}{2}\sum_{\ell=1}^{n}(Z_\ell + (-1)^\ell)\right]^2. \qquad (B4)$$

In this formulation, it is clear that the theory with (θ, L_0) is equivalent to $(\theta + 2\pi L_0, 0)$. Digital quantum simulation in this formulation can be implemented in a similar way to the formulation in the main text. It would be interesting to perform a digital quantum simulation in this formulation and see how this formulation practically works.

APPENDIX C: DETAILS ON QUANTUM SIMULATION PROTOCOL

Here we write down all the qubit operations used in quantum circuits in this paper. First we write down single-qubit operation which acts on a superposition of

$$|0\rangle = \begin{pmatrix} 1 \\ 0 \end{pmatrix} \quad \text{and} \quad |1\rangle = \begin{pmatrix} 0 \\ 1 \end{pmatrix}. \qquad (C1)$$

Some of most basic operations are Pauli matrices:

$$X = \begin{pmatrix} 0 & 1 \\ 1 & 0 \end{pmatrix}, \quad Y = \begin{pmatrix} 0 & -i \\ i & 0 \end{pmatrix}, \quad Z = \begin{pmatrix} 1 & 0 \\ 0 & -1 \end{pmatrix} \qquad (C2)$$

In terms of (X, Y, Z), we also use

$$R_X(\phi) = e^{-\frac{i\phi}{2}X}, \quad R_Y(\phi) = e^{-\frac{i\phi}{2}Y}, \quad R_Z(\phi) = e^{-\frac{i\phi}{2}Z}. \qquad (C3)$$

The only two-qubit operation used in this paper is controlled X (controlled-NOT):

$$CX = \begin{pmatrix} 1 & 0 & 0 & 0 \\ 0 & 1 & 0 & 0 \\ 0 & 0 & 0 & 1 \\ 0 & 0 & 1 & 0 \end{pmatrix} = \begin{array}{c} \bullet \\ \oplus \end{array} \qquad (C4)$$

which acts on superposition of $|i\rangle \otimes |j\rangle$ with $i, j = 0, 1$. In particular, CX satisfies

$$CX|0\rangle \otimes |\alpha\rangle = |0\rangle \otimes |\alpha\rangle, \quad CX|1\rangle \otimes |\alpha\rangle = |1\rangle \otimes X|\alpha\rangle. \qquad (C5)$$

We can construct all the operators in (23) by combinations of the quantum elementary gates $R_{X,Y,Z}$ and CX. First, $e^{-iH_Z\delta t}$ is simply realized by a product of single-qubit operations:

$$e^{-iH_Z\delta t} = \prod_{n=1}^{N} R_Z^{(n)}(2c_n\delta t), \qquad (C6)$$

where $R_Z^{(n)}(\phi)$ stands for a $R_Z(\phi)$ gate acting on the nth qubit and c_n is defined by $\sum_{n=1}^N c_n Z_n = H_{Z,A}(t)$. The other two unitary operators in (23) involve two-qubit operations. The operator $e^{-iH_{ZZ}\delta t}$ needs the following two-qubit operations of

$$e^{-i\frac{J\delta t}{2}Z_1 Z_2},\qquad\qquad (C7)$$

to appropriate pairs of qubits. This operator is the same as the interaction of the Ising model and its concrete realization is

$$e^{-i\frac{J\delta t}{2}Z_1 Z_2} = CX^{(12)}R_Z^{(2)}(J\delta t)CX^{(12)},\qquad (C8)$$

with a quantum gate given by

$$\qquad\qquad (C9)$$

The operator $e^{-iH_\pm\frac{t\delta t}{T}}$ can be constructed in a similar way. It needs the two-qubit operations of

$$e^{-i\frac{\tilde{w}\delta t}{2}(X_1 X_2 + Y_1 Y_2)} = e^{-i\frac{\tilde{w}\delta t}{2}X_1 X_2}e^{-i\frac{\tilde{w}\delta t}{2}Y_1 Y_2} + \mathcal{O}(\delta t^2),\quad (C10)$$

to appropriate pairs. Here, $\tilde{w}$ is defined by $\tilde{w} := \frac{t}{T}w - \frac{(-1)^n}{2}$ $((1 - \frac{t}{T})m_0 + m)\sin(\theta\frac{t}{T})$. This is concretely realized by

$$e^{-i\frac{\tilde{w}\delta t}{2}X_1 X_2} = CX^{(12)}R_X^{(1)}(\tilde{w}\delta t)CX^{(12)},\qquad (C11)$$

$$e^{-i\frac{\tilde{w}\delta t}{2}Y_1 Y_2} = \prod_{j=1}^2 R_Z^{(j)}\left(\frac{\pi}{2}\right)\cdot e^{-i\frac{\tilde{w}\delta t}{2}X_1 X_2}\cdot \prod_{j=1}^2 R_Z^{(j)}\left(-\frac{\pi}{2}\right),\quad (C12)$$

whose circuit diagrams are, respectively, given by

$$\qquad\qquad (C13)$$

$$\qquad\qquad (C14)$$

For example, we implement the time evolution operator $U(t)$ (23) with lattice size $N = 4$ by the following quantum circuit:

$$\qquad\qquad (C15)$$

where the argument of each unitary gate is suppressed and can be read off from (12), (21), and (23): $R_Z^{(n)} \to R_Z^{(n)}(2c_n\delta t)$, $X_n X_{n+1} \to X_n X_{n+1}(\frac{\tilde{w}\delta t}{2})$, $Y_n Y_{n+1} \to Y_n Y_{n+1}(\frac{\tilde{w}\delta t}{2})$, $Z_1 Z_2 \to Z_1 Z_2(J\delta t)$, $Z_1 Z_3 \to Z_1 Z_3(\frac{J\delta t}{2})$, and $Z_2 Z_3 \to Z_2 Z_3(\frac{J\delta t}{2})$.

APPENDIX D: ESTIMATION OF SYSTEMATIC ERRORS

Here we explain how we estimate systematic errors shown in the main text. A VEV of an operator $\mathcal{O}$ is defined by

$$\langle\mathcal{O}\rangle = \langle 0|\mathcal{O}|0\rangle,\qquad\qquad (D1)$$

where here we denote ground state of a system under consideration by $|0\rangle$. Suppose we would like to find an approximation of this quantity by using an adiabatic preparation of the vacuum as in the main text. Let us denote the approximate vacuum obtained in this way as $|0_A\rangle$. Then, we approximate the VEV (D1) by

$$\langle\mathcal{O}\rangle_A = \langle 0_A|\mathcal{O}|0_A\rangle,\qquad\qquad (D2)$$

which is generically different from the true VEV. The state $|0_A\rangle$ can be expanded as

$$|0_A\rangle = \sum_{n=0}^{\infty} c_n |n\rangle, \tag{D3}$$

where $|n\rangle$ is the nth excited state of the full Hamiltonian H of the system. If we take the adiabatic time T and the number of steps M in the Suzuki-Trotter decomposition sufficiently large, then we expect $|c_0| \simeq 1 \gg |c_{n\neq 0}|$ and $|0_A\rangle$ is almost the true vacuum.

Now we propose how to estimate systematic error in approximating the VEV (D1) by (D2). Let us consider the quantity

$$\langle \mathcal{O} \rangle_A(t) = \langle 0_A | e^{iHt} \mathcal{O} e^{-iHt} | 0_A \rangle. \tag{D4}$$

If we managed to prepare the vacuum exactly, i.e., $|0\rangle_A = |0\rangle$, then this quantity was reduced to $\langle \mathcal{O} \rangle$ and independent of t since the vacuum is the eigenstate of H. However, this quantity depends on t when we have only approximation of the vacuum. Let us see how it depends on t using the expansion (D3):

$$\langle \mathcal{O} \rangle_A(t) = \sum_{n=0}^{\infty} |c_n|^2 \langle n|\mathcal{O}|n\rangle$$
$$+ 2\sum_{m\neq n} \text{Re}(c_m^* c_n e^{i(E_m - E_n)t} \langle m|\mathcal{O}|n\rangle), \tag{D5}$$

which implies that this quantity oscillates around the constant $\sum_{n=0}^{\infty} |c_n|^2 \langle n|\mathcal{O}|n\rangle$ as varying t. If we have a nice approximation of the vacuum such that $|c_0| \gg |c_{n\neq 0}|$, then we approximately have

$$\langle \mathcal{O} \rangle_A(t) \simeq |c_0|^2 \left[\langle \mathcal{O} \rangle + \sum_{n=1}^{\infty} \text{Re}\left(\frac{2c_n^* c_0}{|c_0|^2} e^{i(E_n - E_0)t} \langle n|\mathcal{O}|0\rangle \right) \right.$$
$$\left. + \mathcal{O}\left(\left| \frac{c_n}{c_0} \right|^2 \right) \right], \tag{D6}$$

which approximately oscillates around $\simeq \langle \mathcal{O} \rangle$. Therefore, the quantity $\langle \mathcal{O} \rangle_A(t)$ represents intrinsic ambiguity in predicting the true VEV $\langle \mathcal{O} \rangle$ by the adiabatic state preparation. Thus, in the main text, we regard

$$\frac{1}{2}(\max\langle \mathcal{O} \rangle_A(t) + \min\langle \mathcal{O} \rangle_A(t)) \tag{D7}$$

as central value, and

$$\frac{1}{2}(\max\langle \mathcal{O} \rangle_A(t) - \min\langle \mathcal{O} \rangle_A(t)) \tag{D8}$$

as systematic error in approximating the true VEV $\langle \mathcal{O} \rangle$ by the adiabatic preparation of the vacuum.

Figure 5 demonstrates the above procedure for the VEV of the mass operator computed in the main text. In Fig. 5 (left), we fix the Trotter step to $\delta t = 0.1$ and plot the results
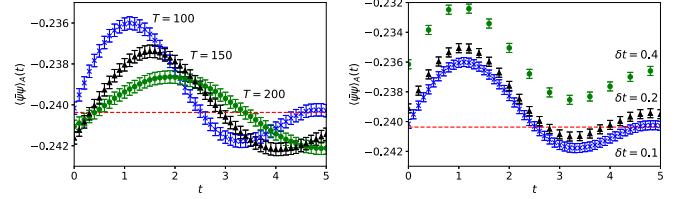

FIG. 5. The expectation value of the mass operator under the state $e^{-iHt}|0_A\rangle$ for $(g, m, N, w) = (1, 0, 4, 0.5)$ against t obtained by simulations with $m_0 = 0.5$ and 10^6 shots. The red dashed line is the result obtained by diagonalization of the Hamiltonian. The error bars are statistical errors. (Left) At fixed $\delta t = 0.1$ with some values of T. (Right) At fixed $T = 100$ with some values of δt

for different values of the adiabatic time T. We find that the expectation value of the mass operator under the state $e^{-iHt}|0_A\rangle$ oscillates around the true VEV obtained of the Hamiltonian as expected. We also find that the result with larger T has smaller amplitude. This reflects the fact that the approximate vacuum $|0_A\rangle$ with larger T is closer to the true vacuum and therefore the systematic error must be smaller for larger T. In Fig. 5 (right), we fix T as $T = 100$ and plot the results for different values of δt. The green circles show that if we do not take sufficiently small δt, then approximation of the time-evolution operator e^{-iHt} breaks down and it does not oscillate around the correct value. In Fig. 6, the adiabatic time dependence of the systematic errors associated with the mass operator is shown for different fermion masses and θ values. All the curves are roughly proportional to $1/T$. It nicely shows that the smaller fermion mass or larger θ result in larger systematic errors. Thus, it is important to take appropriate values of T and δt to get reasonable approximations.

Finally, we comment on the potential reduction of the number of Trotter steps. One can actually tell from Fig. 5 that $10^4 \sim 10^5$ shots would be enough to maintain the same order of the total error. For instance, if we decrease the number of shots to 10^4, the statistical error is roughly 10 times larger, whose magnitude is comparable to the adiabatic error.
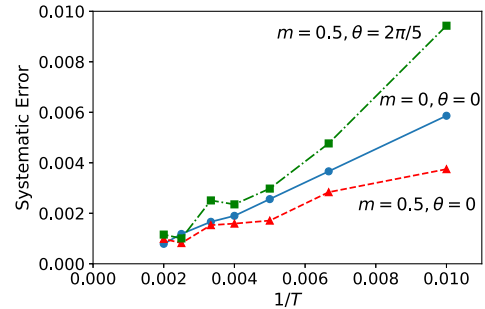

FIG. 6. The systematic errors of the mass operator under the state $e^{-iHt}|0_A\rangle$ for $(g, N, w) = (1, 8, 0.5)$ against the inverse adiabatic time $1/T$ obtained by simulations with 10^6 shots. All the data points are obtained by exact time evolution of the Hamiltonian without the Trotter decomposition.

APPENDIX E: IMPROVEMENT OF THE SUZUKI-TROTTER DECOMPOSITION

The first-order Suzuki-Trotter decomposition is

$$e^{-i(H_1+H_2)\delta t} = e^{-iH_1\delta t}e^{-iH_2\delta t} + \mathcal{O}(\delta t^2), \qquad (E1)$$

for noncommuting operators H_1 and H_2. This error is reduced by using the second-order decomposition,

$$e^{-i(H_1+H_2)\delta t} = e^{-iH_1\frac{\delta t}{2}}e^{-iH_2\delta t}e^{-iH_1\frac{\delta t}{2}} + \mathcal{O}(\delta t^3). \quad (E2)$$

Let us apply this improvement to our adiabatic state preparation. First we decompose the adiabatic Hamiltonian as

$$H_A(t) = \tilde{H}_Z(t) + \tilde{H}_X(t) + \tilde{H}_Y(t), \qquad (E3)$$

where

$$\tilde{H}_Z = H_{ZZ} + H_{Z,A}(t)$$
$$\tilde{H}_X = \frac{1}{2}\sum_{n=1}^{N-1} h_{XY}(t)X_n X_{n+1},$$
$$\tilde{H}_Y = \frac{1}{2}\sum_{n=1}^{N-1} h_{XY}(t)Y_n Y_{n+1},$$
$$h_{XY}(t) = \frac{t}{T}w - \frac{(-1)^n}{2}\left[\left(1-\frac{t}{T}\right)m_0 + \frac{t}{T}m\right]\sin\left(\frac{t}{T}\theta\right). \quad (E4)$$

This implies that the Hamiltonian can be divided into three sets of operators:

$$\tilde{H}_Z : \{Z_1, ..., Z_N, Z_1 Z_2, Z_1 Z_3, ..., Z_{N-1} Z_N\},$$
$$\tilde{H}_X : \{X_1 X_2, X_2 X_3, ..., X_{N-1} X_N\},$$
$$\tilde{H}_Y : \{Y_1 Y_2, Y_2 Y_3, ..., Y_{N-1} Y_N\}. \qquad (E5)$$

The operators commute with each other within each set. Then, the time evolution operator $U(t) = e^{-iH_A(t)\delta t}$ is approximated by

$$U(t) = e^{-i\tilde{H}_Y\frac{\delta t}{2}}e^{-i\tilde{H}_X\frac{\delta t}{2}}e^{-i\tilde{H}_Z\delta t}e^{-i\tilde{H}_X\frac{\delta t}{2}}e^{-i\tilde{H}_Y\frac{\delta t}{2}} + \mathcal{O}(\delta t^3). \quad (E6)$$

In this improvement, the quantum circuit for 16 qubits has about 400 single-qubit gates and 500 two-qubit gates at each time step while the one without the improvement has 250 single-qubit gates and 270 two-qubit gates. Note that the improvement saves the number of gates in the total time evolution since it needs smaller time steps to achieve the same accuracy.

[1] C. Ratti, Lattice QCD and heavy ion collisions: A review of recent progress, Rep. Prog. Phys. **81**, 084301 (2018).

[2] H.-W. Lin, Review of baryon spectroscopy in lattice QCD, Chin. J. Phys. **49**, 827 (2011).

[3] O. Philipsen, The QCD equation of state from the lattice, Prog. Part. Nucl. Phys. **70**, 55 (2013).

[4] H.-T. Ding, F. Karsch, and S. Mukherjee, Thermodynamics of strong-interaction matter from Lattice QCD, Int. J. Mod. Phys. E **24**, 1530007 (2015).

[5] T. Izubuchi, S. Aoki, K. Hashimoto, Y. Nakamura, T. Sekido, and G. Schierholz, Dynamical QCD simulation with theta terms, Proc. Sci., LATTICE2007 (**2007**) 106.

[6] G. Aarts, Introductory lectures on lattice QCD at nonzero baryon number, J. Phys. Conf. Ser. **706**, 022004 (2016).

[7] S. Takeda, Tensor network approach to real-time path integral, Proc. Sci., LATTICE2019 (**2019**) 033.

[8] J. Preskill, Quantum computing and the entanglement frontier, arXiv:1203.5813.

[9] F. Arute *et al.*, Quantum supremacy using a programmable superconducting processor, Nature (London) **574**, 505 (2019).

[10] J. S. Schwinger, Gauge invariance and mass, Phys. Rev. **125**, 397 (1962).

[11] S. R. Coleman, R. Jackiw, and L. Susskind, Charge shielding and quark confinement in the massive Schwinger model, Ann. Phys. (N.Y.) **93**, 267 (1975).

[12] S. R. Coleman, More about the massive Schwinger model, Ann. Phys. (N.Y.) **101**, 239 (1976).

[13] N. S. Manton, The Schwinger model and its axial anomaly, Ann. Phys. (N.Y.) **159**, 220 (1985).

[14] J. E. Hetrick and Y. Hosotani, QED on a circle, Phys. Rev. D **38**, 2621 (1988).

[15] J. E. Hetrick, Y. Hosotani, and S. Iso, The massive multi—flavor Schwinger model, Phys. Lett. B **350**, 92 (1995).

[16] Y. Hosotani, R. Rodriguez, J. E. Hetrick, and S. Iso, Confinement and chiral dynamics in the multiflavor Schwinger model, in *Continuous advances in QCD 1996, Proceedings, Conference, Minneapolis, USA, 1996* (1996), pp. 382–390.

[17] Y. Hosotani, Gauge theory model: Quark dynamics and antiferromagnets, in *Physics. Proceedings, 2nd International A. D. Sakharov Conference, Moscow, Russia, 1996* (1996), pp. 445–449.

[18] C. Adam, Normalization of the chiral condensate in the massive Schwinger model, Phys. Lett. B **440**, 117 (1998).

[19] C. Adam, Massive Schwinger model within mass perturbation theory, Ann. Phys. (N.Y.) **259**, 1 (1997).

[20] J. Preskill, Quantum Computing in the NISQ era and beyond, Quantum **2**, 79 (2018).

[21] S. P. Jordan, K. S. M. Lee, and J. Preskill, Quantum algorithms for quantum field theories, Science **336**, 1130 (2012).

[22] S. P. Jordan, K. S. M. Lee, and J. Preskill, Quantum computation of scattering in scalar quantum field theories, Quantum Inf. Comput. **14**, 1014 (2014).

[23] S. P. Jordan, K. S. M. Lee, and J. Preskill, Quantum algorithms for fermionic quantum field theories, arXiv:1404 .7115.

[24] L. García-Álvarez, J. Casanova, A. Mezzacapo, I. L. Egusquiza, L. Lamata, G. Romero, and E. Solano, Fermion-Fermion Scattering in Quantum Field Theory with Superconducting Circuits, Phys. Rev. Lett. **114**, 070502 (2015).

[25] U.-J. Wiese, Towards quantum simulating QCD, Nucl. Phys. **A931**, 246 (2014).

[26] D. Marcos, P. Widmer, E. Rico, M. Hafezi, P. Rabl, U. J. Wiese, and P. Zoller, Two-dimensional lattice gauge theories with superconducting quantum circuits, Ann. Phys. (Amsterdam) **351**, 634 (2014).

[27] A. Mezzacapo, E. Rico, C. Sabín, I. L. Egusquiza, L. Lamata, and E. Solano, Non-Abelian $SU(2)$ Lattice Gauge Theories in Superconducting Circuits, Phys. Rev. Lett. **115**, 240502 (2015).

[28] E. A. Martinez *et al.*, Real-time dynamics of lattice gauge theories with a few-qubit quantum computer, Nature (London) **534**, 516 (2016).

[29] C. Muschik, M. Heyl, E. Martinez, T. Monz, P. Schindler, B. Vogell, M. Dalmonte, P. Hauke, R. Blatt, and P. Zoller, U(1) Wilson lattice gauge theories in digital quantum simulators, New J. Phys. **19**, 103020 (2017).

[30] A. Macridin, P. Spentzouris, J. Amundson, and R. Harnik, Electron-Phonon Systems on a Universal Quantum Computer, Phys. Rev. Lett. **121**, 110504 (2018).

[31] H. Lamm and S. Lawrence, Simulation of Nonequilibrium Dynamics on a Quantum Computer, Phys. Rev. Lett. **121**, 170501 (2018).

[32] N. Klco and M. J. Savage, Digitization of scalar fields for quantum computing, Phys. Rev. A **99**, 052335 (2019).

[33] N. Klco, E. F. Dumitrescu, A. J. McCaskey, T. D. Morris, R. C. Pooser, M. Sanz, E. Solano, P. Lougovski, and M. J. Savage, Quantum-classical computation of Schwinger model dynamics using quantum computers, Phys. Rev. A **98**, 032331 (2018).

[34] E. Gustafson, Y. Meurice, and J. Unmuth-Yockey, Quantum simulation of scattering in the quantum Ising model, Phys. Rev. D **99**, 094503 (2019).

[35] A. Alexandru, P. F. Bedaque, H. Lamm, and S. Lawrence (NuQS Collaboration), σ Models on Quantum Computers, Phys. Rev. Lett. **123**, 090501 (2019).

[36] N. Klco and M. J. Savage, Minimally-entangled state preparation of localized wavefunctions on quantum computers, Phys. Rev. A **102**, 012612 (2020).

[37] N. Klco, J. R. Stryker, and M. J. Savage, SU(2) non-Abelian gauge field theory in one dimension on digital quantum computers, Phys. Rev. D **101**, 074512 (2020).

[38] H. Lamm, S. Lawrence, and Y. Yamauchi (NuQS Collaboration), Parton physics on a quantum computer, Phys. Rev. Research **2**, 013272 (2020).

[39] G. Magnifico, M. Dalmonte, P. Facchi, S. Pascazio, F. V. Pepe, and E. Ercolessi, Real time dynamics and confinement in the $\mathbb{Z}_n$ Schwinger-Weyl lattice model for $1+1$ QED, Quantum **4**, 281 (2020).

[40] N. Mueller, A. Tarasov, and R. Venugopalan, Deeply inelastic scattering structure functions on a hybrid quantum computer, Phys. Rev. D **102**, 016007 (2020).

[41] E. Gustafson, P. Dreher, Z. Hang, and Y. Meurice, Real time evolution of a one-dimensional field theory on a 20 qubit machine, Quantum Sci. Technol. **6**, 045020 (2021).

[42] E. Zohar, J. I. Cirac, and B. Reznik, Simulating Compact Quantum Electrodynamics with Ultracold Atoms: Probing Confinement and Nonperturbative Effects, Phys. Rev. Lett. **109**, 125302 (2012).

[43] D. Banerjee, M. Dalmonte, M. Muller, E. Rico, P. Stebler, U. J. Wiese, and P. Zoller, Atomic Quantum Simulation of Dynamical Gauge Fields coupled to Fermionic Matter: From String Breaking to Evolution after a Quench, Phys. Rev. Lett. **109**, 175302 (2012).

[44] E. Zohar, J. I. Cirac, and B. Reznik, Cold-Atom Quantum Simulator for SU(2) Yang-Mills Lattice Gauge Theory, Phys. Rev. Lett. **110**, 125304 (2013).

[45] D. Banerjee, M. Bögli, M. Dalmonte, E. Rico, P. Stebler, U. J. Wiese, and P. Zoller, Atomic Quantum Simulation of U (N) and SU(N) Non-Abelian Lattice Gauge Theories, Phys. Rev. Lett. **110**, 125303 (2013).

[46] U.-J. Wiese, Ultracold quantum gases and lattice systems: Quantum simulation of lattice gauge theories, Ann. Phys. (Amsterdam) **525**, 777 (2013).

[47] E. Zohar, J. I. Cirac, and B. Reznik, Quantum simulations of lattice gauge theories using ultracold atoms in optical lattices, Rep. Prog. Phys. **79**, 014401 (2016).

[48] A. Bazavov, Y. Meurice, S.-W. Tsai, J. Unmuth-Yockey, and J. Zhang, Gauge-invariant implementation of the Abelian Higgs model on optical lattices, Phys. Rev. D **92**, 076003 (2015).

[49] E. Zohar, A. Farace, B. Reznik, and J. I. Cirac, Digital lattice gauge theories, Phys. Rev. A **95**, 023604 (2017).

[50] A. Bermudez, G. Aarts, and M. Müller, Quantum Sensors for the Generating Functional of Interacting Quantum Field Theories, Phys. Rev. X **7**, 041012 (2017).

[51] H. Bernien, S. Schwartz, A. Keesling, H. Levine, A. Omran, H. Pichler, S. Choi, A. S. Zibrov, M. Endres, M. Greiner *et al.*, Probing many-body dynamics on a 51-atom quantum simulator, Nature (London) **551**, 579 (2017).

[52] T. V. Zache, F. Hebenstreit, F. Jendrzejewski, M. K. Oberthaler, J. Berges, and P. Hauke, Quantum simulation of lattice gauge theories using Wilson fermions, Sci. Technol. **3**, 034010 (2018).

[53] J. Zhang, J. Unmuth-Yockey, J. Zeiher, A. Bazavov, S. W. Tsai, and Y. Meurice, Quantum Simulation of the Universal Features of the Polyakov Loop, Phys. Rev. Lett. **121**, 223201 (2018).

[54] H.-H. Lu *et al.*, Simulations of subatomic many-body physics on a quantum frequency processor, Phys. Rev. A **100**, 012320 (2019).

[55] F. M. Surace, P. P. Mazza, G. Giudici, A. Lerose, A. Gambassi, and M. Dalmonte, Lattice Gauge Theories and String Dynamics in Rydberg Atom Quantum Simulators, Phys. Rev. X **10**, 021041 (2020).

[56] C. Kokail *et al.*, Self-verifying variational quantum simulation of lattice models, Nature (London) **569**, 355 (2019).

[57] T. Byrnes, P. Sriganesh, R. J. Bursill, and C. J. Hamer, Density matrix renormalization group approach to the massive Schwinger model, Nucl. Phys. B, Proc. Suppl. **109**, 202 (2002).

[58] B. Buyens, S. Montangero, J. Haegeman, F. Verstraete, and K. Van Acoleyen, Finite-representation approximation of lattice gauge theories at the continuum limit with tensor networks, Phys. Rev. D **95**, 094509 (2017).

[59] Y. Kuramashi and Y. Yoshimura, Tensor renormalization group study of two-dimensional U(1) lattice gauge theory with a θ term, J. High Energy Phys. 04 (2020) 089.

[60] L. Funcke, K. Jansen, and S. Kühn, Topological vacuum structure of the Schwinger model with matrix product states, Phys. Rev. D **101**, 054507 (2020).

[61] T. V. Zache, N. Mueller, J. T. Schneider, F. Jendrzejewski, J. Berges, and P. Hauke, Dynamical Topological Transitions in the Massive Schwinger Model with a θ Term, Phys. Rev. Lett. **122**, 050403 (2019).

[62] C. J. Hamer, W.-h. Zheng, and J. Oitmaa, Series expansions for the massive Schwinger model in Hamiltonian lattice theory, Phys. Rev. D **56**, 55 (1997).

[63] K. Fujikawa, Path Integral Measure for Gauge Invariant Fermion Theories, Phys. Rev. Lett. **42**, 1195 (1979).

[64] J. B. Kogut and L. Susskind, Hamiltonian formulation of Wilson's lattice gauge theories, Phys. Rev. D **11**, 395 (1975).

[65] L. Susskind, Lattice Fermions, Phys. Rev. D **16**, 3031 (1977).

[66] P. Jordan and E. Wigner, Über das paulische äquivalenzverbot, Z. Phys. **47**, 631 (1928).

[67] S. Lloyd, Universal quantum simulators, Science **273**, 1073 (1996).

[68] M. Suzuki, General theory of fractal path integrals with applications to manybody theories and statistical physics, J. Math. Phys. (N.Y.) **32**, 400 (1991).

[69] M. Luscher, Computational Strategies in Lattice QCD, in *Modern perspectives in lattice QCD: Quantum field theory and high performance computing, Proceedings, International School, 93rd Session, Les Houches, France, 2009* (2010), pp. 331–399.

[70] M. C. Bañuls, K. Cichy, K. Jansen, and H. Saito, Chiral condensate in the Schwinger model with matrix product operators, Phys. Rev. D **93**, 094512 (2016).

[71] D. J. Gross, I. R. Klebanov, A. V. Matytsin, and A. V. Smilga, Screening versus confinement in $(1 + 1)$-dimensions, Nucl. Phys. **B461**, 109 (1996).